Inherent strength of grain boundaries in tungsten

I. M. Mikhailovskij,* T. I. Mazilova, V. N. Voyevodin, and A. A. Mazilov
Department of Condensed Matter, National Science Center, Kharkov Institute of Physics and Technology, Akademicheskaja, 1, Kharkov 61108, Ukraine

(Received 10 December 2010; revised manuscript received 21 February 2011; published 15 April 2011)

Grain boundary engineering represents a prospective tool for producing high performance structural and functional materials, including super-strong nanocrystalline materials. There remains a fundamental challenge to experimentally evaluate the inherent strength of grain boundaries providing a higher limit for the strength of polycrystals. Here we report that using a combination of atomic-scale and crystallographic characterizations and *in situ* hydrostatic tests in a field-ion microscope, the inherent strength of grain boundaries can be directly measured. It was found that mechanically annealed dislocation-free tungsten bicrystals having nanometer-sized dimensions are capable of withstanding extreme stresses close to the values of the theoretical strength of monocrystals. This finding provides a guideline for understanding the fundamental mechanical response of nanocrystals relevant to applications.

DOI: 10.1103/PhysRevB.83.134115 PACS number(s): 61.72.Mm, 62.40.+i, 61.66.−f

I. INTRODUCTION

Grain boundaries (GBs), which are the longest known intrinsic structural defects in solids, exert profound effects on the macroscopic behavior of a wide range of polycrystalline materials.[1–4] The reduced cohesion of GBs is usually the controlling factor limiting strength of engineering structural materials. On the other hand, nanocrystalline materials exhibit a variety of unique physical and mechanical properties due to grain-size refinement associated with an increase in the amount of GBs. For nanocrystalline materials the role of GBs is amplified due to the hugely increased fraction of atoms near interfaces. Improving the mechanical properties of polycrystals by increasing the fraction of coincidence site lattice (CSL) grain boundaries with a low reciprocal density of coincident sites Σ is the quintessence of the concept of grain boundary engineering.[5] Recent theoretical studies[6,7] indicate that an upper limit of GB strength is drastically larger than known experimental data. While some important features of the basic mechanical properties of mathematically simulated GBs were revealed, there remains a long-term problem of the experimental determination of the intrinsic strength of GBs.

Using the concept of stress and strength introduced by Galileo in 1638,[8] Mariotte[9,10] made it clear that size effect must occur because the local strength is statistically random and its lowest value encountered in a structure depends on the specimen size: smaller is stronger. In the late 1950s Brenner performed tensile tests on a variety of defect-free whiskers a few microns in diameter, which exhibited strong size effects.[11] The greatest strength in Brenner's experiments is found for individual "unique" specimens, while most whiskers posses less strength, yet still considerably exceeding the strength of conventional material. The first observations of ultrastress phenomena at the nanoscale in needle-shaped specimens[12–15] were made using the field-ion microscope (FIM). As has been shown in these experiments with nanocrystals subjected to a high-electric field in the chamber of a FIM, most of the dislocation-free samples fractured at stresses close to the values of the theoretical strength of solids. One of the frequently appearing at the nanoscale phenomena was strongly pronounced dislocation exhaustion: "the great majority of dislocations present in FIM specimens are removed under the influence of the field" induced stresses.[16] The analogical process known as mechanical annealing is a general size-scale phenomenon proved in different ultrastrength experiments.[17,18] In this regard, mechanical annealing can be used for manufacturing of dislocation-free nanobicrystals available for the high-field treatment at the GPa level of stress. The FIM, which has made it possible to directly observe the atomic structure of bicrystals under well-controlled crystallographic conditions combined with *in situ* mechanical loading, represents a unique technique for illuminating the basic mechanical properties of grain boundaries. It is demonstrated here that, in clear contrast to what has been reported earlier for grain boundaries in metals, the strength of nanobicrystals formed from polycrystalline tungsten wires approach their computed ideal values.

II. EXPERIMENT

The hydrostatic strength of GBs was determined using a high-field test of nanoscale needle-shaped samples. The ultrastress phenomena in nanobicrystals have been studied using a two chamber field-ion microscope.[19] All nanotips were prepared from the same lot of 99.98% pure nonsag tungsten wires (150 μm diameter) with the $\langle 110 \rangle$ axial texture. The drawn W wires were annealed at 1270 K for 10 min in a vacuum of 10^{-6}–10^{-7} Pa. The annealed wire had a fibrous structure with an average fiber size of about 250 nm in diameter. The FIM observations have shown that annealing at 1270 K does not change the average grain size and the misorientation angle distribution of grains. The annealing has caused the growth of GB facets and reduced the linear density of nanofacets from 2×10^8 down to 4×10^7 m^{-1}.[20] Needle-shaped specimens with an initial radius of the curvature of about 15 nm at a hemispherical top were prepared by electrochemically etching the wires in 1 N NaOH solution at ac voltage of 5–8 V. The specimen surface was cleaned and polished *in situ* by the methods of field desorption and by low-temperature field evaporation. Conventional needle-shaped samples have thicknesses near the top ranging from 30 to 70 nm and

effective gauge lengths of the order of a micrometer. The taper angle of specimens was in the range 2°–10°. The experiments were performed in a low-temperature FIM with the samples cooled to 77 K. The residual-gas pressure in the working chamber of the microscope was equal to 10^{-6} Pa and the imaging gas (helium) pressure was equal to 2×10^{-3} Pa. After placement in the microscope, needle-shaped samples were subjected to field evaporation until a mesascopically smooth tip was formed. The tips are atomically smooth and may be described by an axisymmetric curved surface $r = R(z)$ in cylindrical coordinates, where the z direction is the specimen axis. Field ion images were normally obtained in a voltage range 2–22 kV.

Mechanical loading resulted from the application of total voltage equal to the constant voltage V_c corresponding to the threshold field for evaporation and the pulse voltage V_p. The evaporation fields F_c of tungsten from its [110] atomic planes at 77 K is 57 V/nm. The average field strength under the high-field loading of a specimen is given by[16]

$$\langle F\rangle = \frac{\langle F_c\rangle\,(V_c + V_p)}{V_c}. \qquad (1)$$

A pulse generator with a pulse width of 1.5×10^{-7} s at the level of 80% of the amplitude V_p was used. The voltage pulse was varied from 0.5 to 10 kV. Electric field strength can be measured in a helium-operated FIM within a range of about 3%. The nature of FIM projection preserves crystallographic symmetry of the original specimen. Thus, crystallographic information at the nanoscale can be extracted from FIM micrographs in a straightforward manner. Standard stereographic FIM methods were used to measure the orientation relationships of GBs.[16] The accuracy on the misorientation angle determination for high-angle grain boundaries is ±2°. The measurement of the GB plane orientation is made with an accuracy of less than 4°.

III. RESULTS AND DISCUSSION

Effective dislocation starvation was performed by field-induced loading under the continuous slow-rising voltage conditions corresponding to a constant rate of field evaporation of about 10^{-2}–10^{-1} nm/s. The average processing time was about 1 h. The electric field strength F corresponding to such a rate of evaporation of tungsten at 77 K is 57±1.5 V/nm. An electric field applied to a metal tip produces a surface mechanical stress[16]

$$\sigma_s = \varepsilon_0 F^2/2, \qquad (2)$$

where ε_0 is the electric constant. The stress related to $F =$ 57 V/nm equals 14.38 GPa.

The surface stress due to electric field acts normal to the surface element at any point. The stress distribution inside the crystal interior is rather complex and consists of both normal σ_n and shear components.[16] For the tips are atomically smooth and may be described by an axisymmetric curved surface $r = R(z)$ in cylindrical coordinates, where the z direction is the specimen axis. For a field evaporated needle-shaped specimen with apex radius r_0, the stress state near the tip surface is virtually hydrostatic. *In situ* deformation

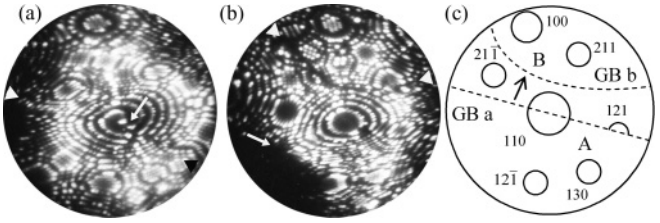

FIG. 1. FIM images of the near-CSL high-angle grain boundary in tungsten. (a) The nanobicrystal before deformation under the triaxial stress of 14.4 GPa. The arrow denotes grain-boundary dislocations $\frac{1}{2}$[110]. (b) The bicrystal after sharp local sliding and low-temperature stress-induced GB migration. The arrow shows the traces of the (112) slip plane; the grain boundary is indicated with arrowheads. (c) Stereographic projection of the bicrystal with the GB before and after migration (shown by arrow).

of nanobicrystals in our experiments corresponded to isotropic (hydrostatic) loading and $\sigma_n \approx \sigma_s$ in this region ($z < r_0$). Isotropic triaxial tension occurs in the vicinity of some lattice defects in solids, for example, voids, cracks, grain, and phase boundaries. Knowledge of the inherent strength of grain boundaries at isotropic tension should greatly contribute to the understanding and designing of mechanical properties of polycrystal materials. However, because of the difficulties in experimental realization of hydrostatic tensile loading, there are no experimental data for isotropic tensile strength and atomistic simulations remain the only relevant means to gain such information.[21]

The grain-boundary resistance against mechanical failure was studied for 93 mechanically annealed tungsten bicrystals under an isotropic tensile load. After the mechanical annealing at $\sigma_n \approx 14.4$ GPa for 1 h, nanobicrystals usually did not contain any lattice dislocation in the gauge region. However, it should be noted that about a half of the specimens broke during such a treatment. Figure 1(a) demonstrates the FIM image of a tungsten bicrystal of 32 nm diameter formed by field evaporation at voltage $U = 4.56$ kV. This characteristic image of a perfect bicrystal consists of bright spots arranged in intersecting sets of concentric rings related to the terraces of close-packed atomic planes. There is no spiral ramps characteristic of dislocations at their points of emergence. Such FIM images correspond to the perfect bicrystals free of dislocations, stacking faults, and nanocracks. They were typical of about 5000 sections obtained by atom-by-atom field evaporation of the tungsten nanobicrystals.

Figures 1(a) and 1(b) are typical FIM images of a high-angle GB in the mechanically annealed tungsten bicrystal. Crystallographic FIM analysis demonstrated that most GBs in studied bicrystals are incoherent boundaries. In spite of the preceding annealing of the drawn W wires at 1270 K, the GB had numerous atomic facets and grain-boundary dislocations [shown by an arrow in Fig. 1(a)], suggesting that such a GB is of a nonequilibrium nature. As in case of super-strong nanocrystalline tungsten,[22] the GB is clean and atomically sharp. There had been no sign of GB phases, amorphous GB regions, or nanocracks. The Burgers vector of grain-boundary dislocations is $\frac{1}{2}$[110]; the dislocation line is parallel to the [110] axis of misorientation. The GB dislocations

correspond neither to the basis vectors of the displacement shift complete nor that of the conventional bcc lattice.[1] Hence, such dislocations are the partial screw GB dislocations. No post-mortem FIM examination of nanobicrystals has ever revealed stacking faults in the vicinity of GBs, suggesting that only perfect lattice dislocations mediate the plasticity as they can be emitted by the boundaries without leaving any planar debris in the bulk regions.

Failure of tungsten nanobicrystals in FIM usually initiates a destructive electrical breakdown, which is accompanied by increasing the tip diameter by more than an order of magnitude and the formation of microprotrusions at the surface.[23] Determination of the radius of the specimen apex after failure revealed that about 10 μm of specimen (including the tested gauge region) was melted and removed from the tip during electrical breakdown. Hence, a rupture mechanism was difficult to determine on the basis of postmortem FIM examination of nanobicrystals. However, in some cases before grain boundary failure occurred, a significant amount of plasticity can be directly observed. FIM analysis demonstrated that several different deformation mechanisms are operative at the GPa level of stress including grain boundary sliding and emission of dislocations. The most striking phenomenon is the appearance of high-index twinning or GPa-level stress-induced grain-boundary migration observed before for the $\Sigma 11$ (332) CSL boundaries.[24–26] The near-CSL GB shown in Fig. 1 is oriented along the $(\bar{1}1\bar{2})_A/(\bar{1}1\bar{1})_B$ with a misorientation angle θ of 19.5° corresponding to the deviation $\Delta\theta$ of about 1° from the exact coincidence misorientation angle θ_Σ for the $\Sigma 33$ CSL GB. A comparison of Figs. 1(a) and 1(b) shows that during a triaxial tensile test at $\sigma_n \approx 14.4$ GPa a very substantial grain-boundary migration [shown by the arrow in Fig. 1(c)] has taken place. The surface trace of the $\Sigma 33$ tilt GB (indicated by arrowheads) was inhomogeneously shifted in the range of 5–12 nm. Low-temperature stress-induced GB migration can be triggered by reactions between lattice dislocations under the action of high stresses.[24] Spontaneously deformed bicrystal also shows a significant shear offset along the $(11\bar{2})$ slip plane, a mode typical of the dislocation-free tungsten and molybdenum monocrystals at the GPa level of stress.[27,28] The surface trace of this shear offset is shown by the arrow in Fig. 1(b). Despite the large expected number of dislocations propagating on the slip planes within this grain, all dislocations are finally absorbed in GBs and on the surface leaving behind no footprint of a dislocation activity.

Figures 2(a)–2(c) show low-temperature stress-induced GB migration [shown by the arrow in Fig. 2(c)] and concomitant local grain boundary slip under the influence of the field-induced stress at the best FIM image voltage corresponding to $F = 45$ V/nm. The [110] small-angle tilt GB shown in Fig. 2 is oriented along the $(\bar{8}8\bar{1})_A/(\bar{2}2\bar{1})_B$ with a misorientation angle of 14.5°. The stress related to this strength of electric field equals 8.96 GPa. Figure 1(b) illustrates a FIM pattern characterized by the broken image rings along the step locus and a "bright-dark" contrast effect due to material on side of the step shifted with respect to the field-evaporated tip envelope. Atomic-scale field evaporation raises the bright-dark contrast across the small-angle GB [Fig. 2(c)]. This FIM contrast is originated from the materials upward displacement from the tip surface into the region where the probabilities

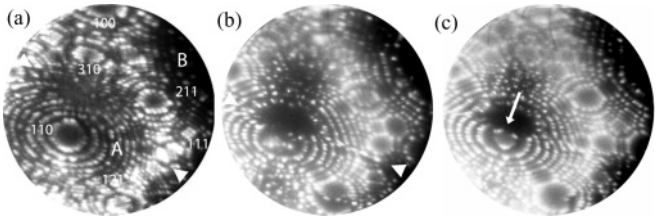

FIG. 2. Stress-induced GB migration and local grain boundary slip under influence of quasistatic GPa-level load. (a) The [110] small-angle tilt GB before deformation under hydrostatic tensile stress of 8.96 GPa; the GB is indicated with arrowheads. (b) The GB after local GB sliding and concomitant stress-induced GB migration. Broken atomic rings along the GB reveal local GB slip. (c) The bright-dark FIM contrast sharpened by fine-scale field evaporation. The arrow shows the direction and magnitude (about 3 nm) of the GB shift.

of field ionization and field evaporation are much higher. The heights of the partly evaporated slip step is equal to three (110) interplanar spacings or 0.67 nm. The step height is given by the total components of the Burgers vector of dislocations which is parallel to the local normal to the surface. Atomically sharp FIM contrast in case of small-angle GB is the evidence of collective glide of the lattice dislocations ($\Sigma = 1$) at the GPa level of tensile stress strictly along the GB planes. Taken as a whole, the FIM observations suggest that tungsten nanobicrystals with an ideal starting atomic structure exhibited unambiguously identified plastic deformation prior to the failure.

We performed both quasistatic and pulse tension tests of the bicrystals at 77 K by applying field-induced hydrostatic static load σ_c of 14.4 GPa and dynamic GPa-level load, respectively. In the quasistatic mode with the slow continuous rising voltage corresponding to a constant rate of field evaporation of about 10^{-2} nm/s, the entire field-induced deformation process and failure in for each sample took about 2 h. The tested GBs were characterized by Brandon's ratio $\Delta\theta/\Delta\theta_{\max}$, where $\Delta\theta$ is the deviation angle from the exact coincidence misorientation angle and $\Delta\theta_{\max}$ is the maximum deviation angle for a specific Σ boundary given by Brandon's criterion defined as $15^\circ/\Sigma^{1/2}$.[5] In quasistatic mode dependence of the total tested volume before failure of the specimen on the misorientation angle was determined.

A total test volume up to failure V_0 of a conical nanotip with the half-angle β subjected to the high-field mechanical testing at a constant hydrostatic stress σ_c is given by[29]

$$V_0 \approx \pi r_0 \left(\frac{2}{3} + \frac{1}{tg\beta}\right). \quad (3)$$

The total test volume is a sum of gauge volume at a given voltage and that of the conic specimen section evaporated during the mechanical testing without failure at the constant field strength and hence the mechanical stress. This total gauge volume may be described in terms of the statistical failure strength distribution as the reference volume corresponding to the given characteristic failure stress level $\sigma_c = 14.4$ GPa close to the theoretical predictions of the GB ideal strength. And vice versa, σ_c is the reference strength for the reference gauge volume V_0.

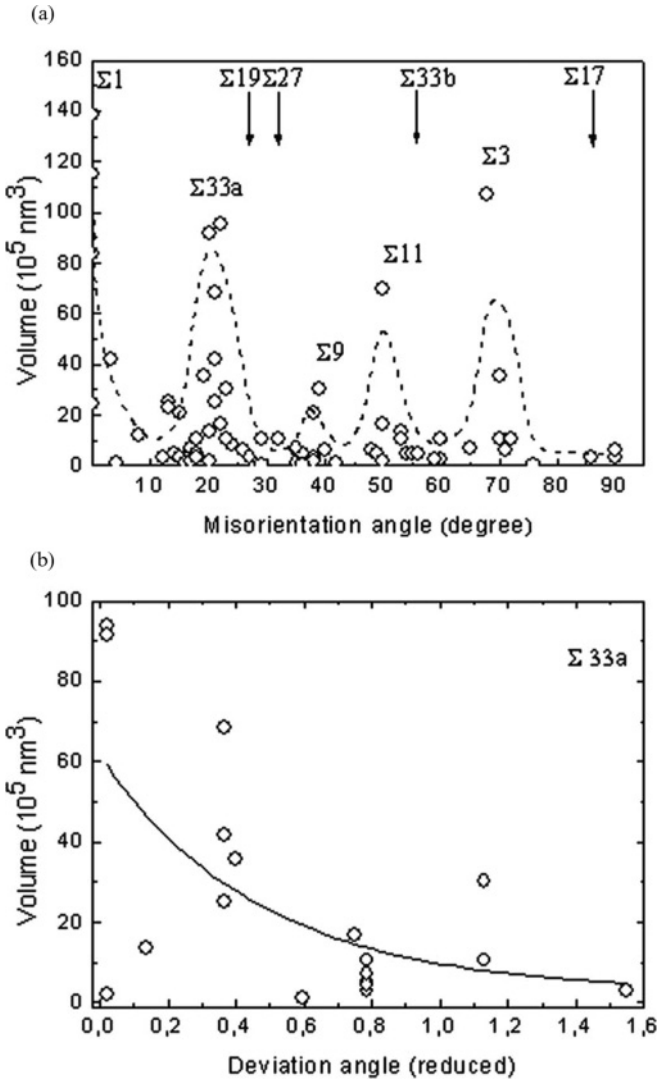

FIG. 3. Resistance of grain boundaries in tungsten to failure for characteristic stress level 14.4 GPa. (a) The reference gauge volume—misorientation angle curve. Arrows denote the positions of exact CSL relations. (b) The dependence of the reference gauge volume on the reduced deviation angle from the exact coincidence misorientation angle for near-Σ33 grain boundaries.

Figure 3(a) shows that some CSL boundaries have the highest reference gauge volume (RGV) compared with the other misorientation studied. This dependence exhibits sharp peaks at certain misorientation angles corresponding to low-Σ CSL misorientations. The maximum RGV for Σ1 corresponds to monocrystalline specimens. The special GBs are classified into two clusters depending on Σ. The Σ1, Σ3, Σ9, and Σ33a grain boundaries possess high resistance to failure. In contrast, no discernible difference in failure resistance is observed between the Σ17, Σ19, Σ27, Σ33b CSL, and random boundaries (RBs). In Fig. 3(b) we illustrate the dependence of the RGV on Brandon's ratio $\Delta\theta/\Delta\theta_{\max}$ for the Σ33 tilt boundaries. Though there is a large data scatter on the reduced deviation angle from exact coincidence misorientation angle $\theta_{\Sigma 33}$, it can be concluded that the RGV for this CSL boundary decreases with increasing Brandon's ratio. Hence, the CSL grain boundaries possess higher resistance to failure than GBs in nearby misorientation angles.

The results of the investigation of the hydrostatic tensile strength of defect-free tungsten bicrystals with RBs [Fig. 4(a)] are presented in Fig. 4(b). The breaking strength at 77 K amounts to 21.5 GPa. This value is nearly independent of the diameter in the investigated range (34–75 nm). The tensile strength of defect-free [110] oriented tungsten monocrystals with the same diameter range is nearly independent of the transverse dimensions and amounted to 31.4 GPa.[14,23] The nanobicrystals with RBs have a rather large average hydrostatic tensile strength σ_0 of 20.2 GPa, which is about 65% of the tensile strength of the defect-free monocrystals. This large critical tensile stress suggests that our nanobicrystals are essentially dislocation-free before testing and consistent with direct FIM observations [Figs. 1, 2, and 4(a)]. There are no GPa-level experimental data known to us on defect-free bicrystals. Earlier experiments on metal bicrystals exhibit a critical stress for GB failure typically less than a few percent of the theoretical tensile strength.[1] For comparison, we have shown in Fig. 4(b) (the dotted region) the data on the uniaxial tensile strength of polycrystalline wires with diameters $D \geqslant 100$ nm prepared by etching tungsten with the ⟨110⟩ axial texture.[30] The strength of the polycrystalline tungsten wire in the large-size asymptotic limit ($\sigma_m \approx 3$ GPa) in Fridman's experiments[30] is nearly equal to the strength of super-strong tungsten with an ultrafine-grain microstructure.[22]

Classical Weibull statistics[10] assumes that the number of flaws is proportional to the volume of the structure, whereas nanocrystals are either defect-free or have a small number of critical flaws. As shown in an asymptotic scaling analysis, a relationship between the strength σ and different sizes D exhibits a two-sided asymptotic support, namely the small- and large-size asymptotic limits. This type of size effect occurs if the crack is initiated at smooth surface (or grain boundary) and there are no preexisting notches. For nanoscale sizes the curves of size effects on the tensile strength deviate from the classical theory fracture due to the fact that the failure process zone size is not negligible compared with the specimen diameter. Our experimental data on the bicrystal strength presented in Fig. 4(b), along with the measured strength of the polycrystalline tungsten wire,[30] can be well fitted by the sigmoidal Weibull function[10]

$$\sigma(D) = \sigma_0 - (\sigma_0 - \sigma_m)\exp\left[-\left(\frac{D}{D^*}\right)^{\beta}\right], \qquad (4)$$

where the best fit give $\sigma_0 = 20.25$ GPa, $\sigma_m = 3.040$ GPa, $D^* = 131.93$ nm, and $\beta = -5.453$.

Although a size effect on the tensile strength of RBs was not observed in the present study, it should be noted that all studied specimens were preliminarily mechanically annealed at $\sigma_n \approx 14.4$ GPa, and about a half of the specimens have been broken during such a treatment. Hence, there was a "natural selection" of strong specimens, which suppressed the data scattering. Nevertheless, the absence of a distinct size effect in the small-size asymptotic range may be due to the attainment in our experiments of the inherent strength which is the intrinsic property of the dislocation-starved bicrystals with RBs. It

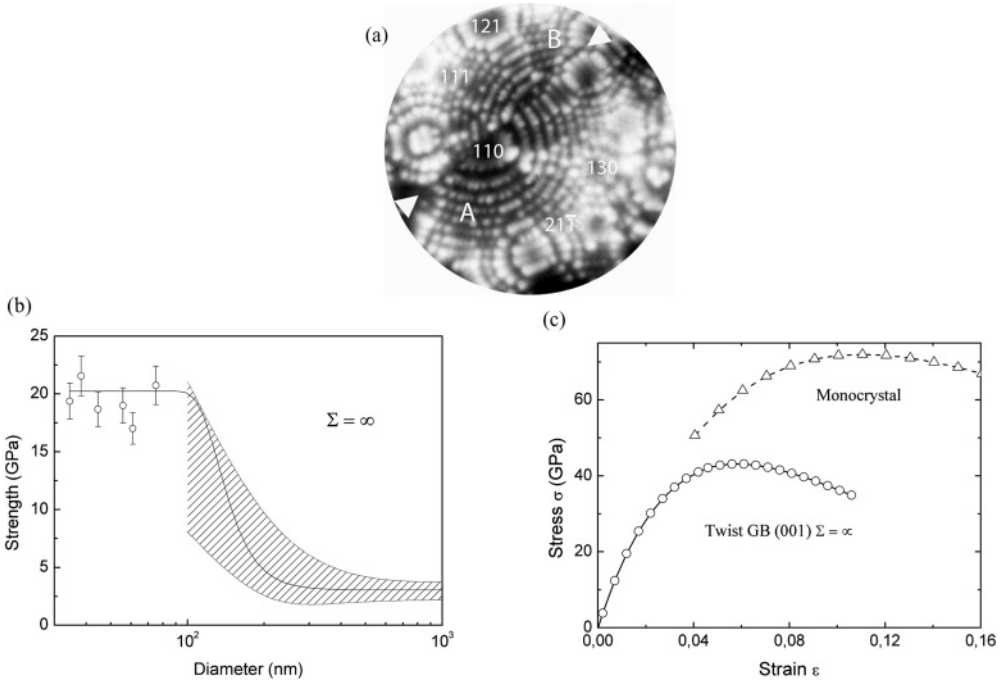

FIG. 4. Hydrostatic tensile strength of defect-free tungsten bicrystals with random GBs. (a) FIM image of the RB. (b) The breaking strength vs diameter of nanotip at 77 K. The dotted region corresponds to Fridman's data.[30] (c) Calculated stress—strain curve of the random twist boundary and tungsten monocrystal.

should be noted, however, that no noticeable difference in the tensile strength in the nanoscale region is observed between the CSL and random boundaries: incoherent (unsymmetrical) twin boundaries $\Sigma 3$ have the average cohesive strength of 22.3 ± 2.2 GPa, which is only about 10% higher than those for RBs.

Since mathematical simulations of GBs almost always employ periodic boundary conditions, it is very complicated to model incommensurate (general) boundaries. These GBs were approximated by near general boundaries ($\Sigma \to \infty$) with long periods.[1] While many atomic simulations of GB failure have been performed, they have usually been confined to CSL boundaries with a high degree of symmetry and with a low Σ value.[6,7] This is also because of the fact that such boundaries exhibit a lower grain boundary energy, which suggests that these boundaries may have unique fracture properties as compared with general (nonsingular) high-angle grain boundaries ($\Sigma = \infty$). However, RBs are more widespread than singular boundaries; they mainly determine the fundamental mechanical response of conventional polycrystals. In this paper the tensile strength of general GBs has been numerically evaluated using a pairwise simulation technique in the reciprocal space (see the Appendix for details). We have considered RBs formed by symmetric lattice rotation around a ⟨100⟩ misorientation axis. Constraints are placed on atoms located on these boundaries to stipulate that these interfaces remain planar and parallel during energy minimization and isotropic tensile deformation processes. In this test the hydrostatic tension was introduced by incrementally stretching the sample a bit along the system axes. This procedure was repeated with increasing strain until the stress level reached the ideal strength. The ideal strength of a grain boundary can be assigned as the maximum stress needed to attain mechanical instability of a bicrystal without introducing cracks or extrinsic lattice dislocations. These calculations correspond to tensile strength determination at zero temperature.

The simulations have showed that elastic deformation of the bicrystal is inhomogeneous and grain boundary atoms are on average strained substantially more than the bulk atoms. A bicrystal deformation matrix can be decomposed into local strain contributions. The contributions to the ε_{zz} component of the strain for grain bulk and grain boundary regions are particularly different. Taking into account that the definition of local strain is not unique in the sense that the effective volume of each atom is not strongly definable, we have used the total strain data for graphic presentation of the stress-strain curves [Fig. 4(c)]. Three-axis tensile stress normal to the RB increases with the increase of strain. At the strain 0.056, tensile stress normal to the boundary reaches its maximum value. Therefore, the theoretical three-axis tensile strength of the (001) W grain boundary with $\Sigma = \infty$ is 43.11 GPa, which is the upper value of tensile strength of this RB. The experimental data in Fig. 4(b) show satisfactory agreement with these calculations of the hydrostatic tensile strength of RBs. A typical discrepancy of about a factor of 2 is observed. There are, unfortunately, no published results for dislocation-free tungsten bicrystals, which should be directly compared with our results. Figure 4(c) shows that the maximum hydrostatic stress at this boundary is substantially lower than that of tungsten monocrystal (72.02 GPa). Nevertheless, the strength of RB is quite large: it is drastically larger than the experimental strength of conventional polycrystals and is about 60% of the theoretical hydrostatic strength of ideal monocrystals.[31]

IV. CONCLUSIONS

Intense effects of grain boundaries on the mechanical properties of polycrystals appear in a wide variety of forms and stem from a wide range of possible sources, including essentially low intergranular cohesion.[1] However, based on our experiments it was found that tungsten polycrystals do not have intrinsically weak grain boundaries. The inherent strength of grain boundaries, including those of a general type, is very much larger than the observed tensile strength of bulk tungsten. In our experiments and simulations nanospecimens contain no inclusions, bulk dislocations, cracks, or defects other than the grain boundaries. In bulk samples the failure stress is controlled by these preexisting flaws, making it impossible to determine the intrinsic yield strength. This is the reason why the failure of conventional materials occurs at stresses far below the ideal strength. It can be claimed that our experimental values are the inherent strengths of grain boundaries without any extrinsic defects. The fracture stresses and strains for the nanobicrystals approach a significant fraction of those theoretical values for the ideal tungsten monocrystals. We believe that a detailed knowledge of basic mechanical properties of grain boundaries should provide a rational pathway for understanding the fundamental mechanical response of ultrafine grained polycrystals and producing super-strong materials.

ACKNOWLEDGMENTS

This work was supported by the Program of the National Academy of Sciences of the Ukraine "Nanosystems, nanomaterials and nanotechnologies" (Grant No. 30/07-H) and the NATO International Program.

APPENDIX : ATOMISTIC MODELING GBS IN RECIPROCAL SPACE

For atomistic simulations of GB resistance to deformation, the structural energy differences are important and the long-range interaction potentials are necessary in order to describe precisely a wide range of local 3D atomic surroundings. Atomistic computer simulations were performed using molecular statics with Morse long-range potential. The thickness of the grain boundary interface model is taken as 31 {100} crystallographic planes (4.74 nm). This thickness is more than seven times larger than the range of the interatomic potential (0.65 nm) corresponding to 1.6% of the well depth for the Morse potential, which is sufficient to preserve the local 3D physics in the simulation cell.[32] The ideal strength corresponding to the maximum in the stress, which occurs at the instability point, was calculated directly by taking a derivative of the energy with respect to the true strain volume. Due to the homogeneous tensile strain and the symmetry of the present cell, all the shear stress components were negligible and can be regarded as zero at the error range. The strength computed here refers to the limit of mechanical stability under quasistatic three-axis deformation in the low-temperature regime.

The analysis in reciprocal space of the interaction between parallel planar atomic nets includes determination of the two-dimensional Fourier transform of the potential by the integrating extended over all two-dimensional space.[1,33] An analytical treatment has no need to limit the range of the pair potential by forcing it to vanish at relatively small separations. To obtain an analytical expression for the energy of interface, the effective pair potential used was

$$v(r) = \sum_p D_p \exp(-\beta_p r), \tag{A1}$$

where r is the distance between atoms and D_p and β_p are adjustable parameters. The potential parameters for W are $D_p =$ 8277 and −181.1 eV and $\beta_p = 2.823$ and 1.412 Å^{-1} for $p =$ 1 and 2, respectively.

It is assumed that the energy of the bicrystal is represented by a sum of pair interactions of atoms in j and k planar atomic layers. Let the lattice sites in these planes be denoted by the sets $\{\vec{X}^j\}$ and $\{\vec{X}^k\}$ and corresponding sets of the reciprocal lattice vectors are $\{\vec{G}^j\}$ and $\{\vec{G}^k\}$. The energy of interaction between two rigid parallel two-dimensional lattices per unit area may be expressed as follows:

$$E_{jk} = \frac{1}{A_j A_k} \sum_{\vec{G}^c} \tilde{v}(\vec{G}^c, z_{jk}) \exp(i\vec{G}^c \cdot \vec{T}_{jk}), \tag{A2}$$

where A_j and A_k are the areas of the primitive unit cells, z_{jk} is the separation between the lattices, $\vec{G}^c$ is a common reciprocal lattice vector, $\vec{T}_{jk}$ denotes an arbitrary relative translation, and $\tilde{v}$ is two-dimensional Fourier transform of the pairwise potential. For an effective potential in form (A1) Fourier transform can be obtained in a closed form[33]:

$$\tilde{v}(G, z_{jk}) = 2\pi \sum_p \frac{\beta_p D_p}{\left(\beta_p^2 + G^2\right)^{3/2}} \left(1 + z_{jk}\sqrt{\beta_p^2 + G^2}\right) \times \exp\left(-z_{jk}\sqrt{\beta_p^2 + G^2}\right). \tag{A3}$$

In order to compute the total energy of the pairwise atomic interaction W a lattice summation must be performed. Within each plane parallel to the grain boundary we use the orthogonal coordinate systems $x - y$. It is assumed that in planar lattices there are no atoms in the crystal basis, but the results will be extended to a general case of base-centered plane parallel to the boundary. The lattice periods in the x and y directions are a_x, a_y, and $|\vec{G}| = \sqrt{g_{xl}^2 + g_{ym}^2}$, where $g_{xl} = \frac{2\pi l}{a_x}$, $g_{ym} = \frac{2\pi m}{a_y}$, and l, m are summation indices locating points in the planar reciprocal lattice. Here a is the parameter of three-dimensional lattice. The module of the relative translation may be expressed as $|\vec{T}_{jk}| = \sqrt{T_{xjk}^2 + T_{yjk}^2}$.

Combining (A2) and (A3) we have

$$W = \pi\sigma^2 \sum_j \sum_{k(\neq j)} \sum_{lm} \sum_p \frac{\beta_p D_p}{q_{plm}^3} (1 + q_{plm}|z_{jk}|) \times \exp(-q_{plm}|z_{jk}|) \cos(g_{xl} T_{xjk}) \cos(g_{ym} T_{yjk}), \tag{A4}$$

where $q_{plm} = \sqrt{\beta_p^2 + g_{xl}^2 + g_{ym}^2}$ and σ is the planar atomic density.

In our computer modeling the position of the rigid atomic planes have been labeled from $-15 < j,k < 15$. The wave-vector numbers were in interval $|l,m| \leqslant 20$, but satisfactory re-

sults for a close-packed boundary may be obtained at less numbers. Only those terms referring to near-surface planes and having both $|l| \leqslant 4$ and $|m| \leqslant 4$ contribute significantly to the sum in W. So the convergence of the series for close-packed atomic planes is high and the method of simulation in reciprocal space is computationally efficient. The RB produced by a rotation of grains about low-indices directions can be obtained by reducing the sets $\{\vec{G}^j\}$ and $\{\vec{G}^k\}$ to $G^j = G^k = 0$ ($l = m = 0$).

*mikhailovskij@kipt.kharkov.ua

[1] A. P. Sutton and R. W. Bulluffi, *Interfaces in Crystalline Materials* (Clarendon, Oxford, 1995).

[2] H.-P. Chen, R. K. Kalia, E. Kaxiras, G. Lu, A. Nakano, K. I. Nomura, A. C. T. van Duin, P. Vashishta, and Z. Yuan, Phys. Rev. Lett. **104**, 155502 (2010).

[3] T. Shimokawa, Phys. Rev. B **82**, 174122 (2010).

[4] S. Malola, H. Häkkinen, and P. Koskinen, Phys. Rev. B **81**, 165447 (2010).

[5] S. Kobayashi, S. Tsurekawa, and T. Watanabe, Acta Mater. **53**, 1051 (2005).

[6] A. Cao, Y. Wei, and E. Ma, Phys. Rev. B **77**, 195429 (2008).

[7] S. Ogata, Y. Umeno, and M. Kohyama, Modelling Simul. Mater. Sci. Eng. **17**, 013001 (2009).

[8] G. Galilei, *Discorsi e Demostrazioni Matematiche, Intorno à due Nuove Scienze* (Elsevirii, Leiden, 1638); G. Galilei, *Dialogues Concerning Two New Sciences,* Trans. H. Crew and A. de Salvio (Amhersts: Prometheus Books, New York, 1991).

[9] E. Mariotte, *Traité du Mouvement des Eaux: Mariotte's Collected Works* (Hague, 1686).

[10] Z. Bažant, PNAS **101**, 13400 (2004).

[11] S. S. Brenner, Science **128**, 569 (1958).

[12] K. D. Rendulic and E. W. Müller, J. Appl. Phys. **37**, 2593 (1966).

[13] E. W. Müller and T. T. Tsong, *Field Ion Microscopy, Principles and Application* (Elsevier, New York, 1969).

[14] I. M. Mikhailovskij, P. Ya. Poltinin, and L. I. Fedorova, Sov. Phys. Solid. State **23**, 757 (1983).

[15] E. F. Talantsev, Supercond. Sci. Technol. **7**, 491 (1994).

[16] M. K. Miller, A. Cerezo, M. G. Hetherington, and G. D. W. Smith, *Atom-Probe Field Ion Microscopy* (Clarendon, Oxford, 1996).

[17] J. R. Greer and W. D. Nix, Phys. Rev. B **73**, 245410 (2006).

[18] Z. W. Shan, R. Mishra, S. A. S. Asif, O. L. Warren, and A. M. Minor, Nature Mater. **7**, 115 (2008).

[19] I. M. Neklyudov, E. V. Sadanov, G. D. Tolstolutskaja, V. A. Ksenofontov, T. I. Mazilova, and I. M. Mikhailovskij, Phys. Rev. B **78**, 115418 (2008).

[20] A. S. Lazarenko, I. M. Mikhailovskij, V. B. Rabukhin and O. A. Velikodnaya, Acta Metall. Mater. **43**, 639 (1995).

[21] M. Černy, J. Pokluda, M. Šob, M. Friak, and P. Šandera, Phys. Rev. B **67**, 035116 (2003).

[22] Q. Wei, H. T. Zhang, B.E. Schuster, K. T. Ramesh, R.Z. Valiev, L. J. Kecskes, R. J. Dowding, L. Magness, and K. Cho, Acta Mater. **54**, 4079 (2006).

[23] I. M. Mikhailovskij, N. Wanderka, V. E. Storizhko, V.A. Ksenofontov, and T.I. Mazilova, Ultramicroscopy **109**, 480 (2009).

[24] Zh. I. Dranova and I. M. Mikhailovskii, Sov. Phys.-Solid State **14**, 3104 (1973).

[25] D. Farkas, Philos. Mag. **85**, 387 (2005).

[26] L. M. Dougherty, G. T. Gray III, E. K. Cerreta, R. J. McCabe, R. D. Field, and J. F. Bingert, Scr. Mater. **60**, 772 (2009).

[27] S. Kotrechko, O. Filatov, and O. Ovsjannikov, Mater. Sci. Forum **567/568**, 65 (2007).

[28] A. P. Shpak, S. O. Kotrechko, T. I. Mazilova, and I. M. Mikhailovskij, Sci. Technol. Adv. Mater. **10**, 045004 (2009).

[29] A. S. Bakai, A. P. Shpak, N. Wanderka, S. Kotrechko, T. I. Mazilova, and I. M. Mikhailovskij, J. Non-Cryst. Solids **356**, 1310 (2010).

[30] V. Ya. Fridman, Sov. Phys.-Solid State **12**, 2461 (1971).

[31] D. Roundy, C. R. Krenn, M. L. Cohen, and J. W. Morris, Philos. Mag. A **81**, 1725 (2001).

[32] L. Shen and Z. Chen, Modelling Simul. Mater. Sci. Eng. **12**, S347 (2004).

[33] V. I. Gerasimenko, T. I. Mazilova, and I. M. Mikhailovskij, Phys. Met. Metallogr. **91**, 335 (2001).